Fusion Engineering and Design 18 (1991) 135–144
North-Holland

Prediction for disruption erosion of ITER plasma facing components; a comparison of experimental and numerical results

J.G. van der Laan [a], M. Akiba [b], A. Hassanein [c], M. Seki [b] and V. Tanchuk [d]

[a] *The NET Team, c/o Max-Planck Institut für Plasmaphysik, Boltzmannstrasse 2, W-8046 Garching, Germany*
[b] *Japan Atomic Energy Research Institute, Naka-machi, Ibaraki-ken, 311-01, Japan*
[c] *Argonne National Laboratory, 9700 South Cass Avenue, Argonne, Illinois 60439, USA*
[d] *D.V. Efremov Institute for Electrophysical Apparatus, Leningrad, 189631, USSR*

An evaluation is given for the prediction for disruption erosion in the International Thermonuclear Engineering Reactor (ITER). At first, a description is given of the relation between plasma operating parameters and system dimensions to the predictions of loading parameters of Plasma Facing Components (PFC) in off-normal events. Numerical results from ITER parties on the prediction of disruption erosion are compared for a few typical cases and discussed. Apart from some differences in the codes, the observed discrepancies can be ascribed to different input data of material properties and boundary conditions. Some physical models for vapour shielding and their effects on numerical results are mentioned. Experimental results from ITER parties, obtained with electron and laser beams, are also compared. Erosion rates for the candidate ITER PFC materials are shown to depend very strongly on the energy deposition parameters, which are based on plasma physics considerations, and on the assumed material loss mechanisms. Lifetimes estimates for divertor plate and first wall armour are given for carbon, tungsten and beryllium, based on the erosion in the thermal quench phase.

1. Introduction

The reference ITER plasma disruption scenario consists of a fast thermal quench followed by a slower current quench phase, with different energy deposition characteristics [1], see fig. 1. In the fast (0.1–3 ms) thermal quench phase of the disruption, 80% of the thermal energy (typically 500 MJ) is lost to the wall by conduction, convection and radiation. It is assumed that half of it goes to one divertor, mainly in the form of particles and half to the first wall. In the subsequent slower (5–50 ms) current quench phase (magnetic) energy is deposited on divertor and first wall by radiation from the strongly contaminated plasma. The highest loads anticipated are on the divertor where 250 MJ is deposited on an area of about 20 m^2, due to an expected 3 times widening of the normal power scrape-off layer, corresponding to actual tokamak experience [1]. This leads to an energy density (E'') of 12 MJ/m^2, without toroidal peaking. The engineering reference values during the ITER Conceptual Design Activity have been 10–20 MJ/m^2 [2]. The fast phase energy deposition on the first wall is expected to be peaked (factor 5) to 2 MJ/m^2 maximum.

The energy deposition during the current quench is estimated to be 2–3 MJ/m^2 maximum on both divertor and first wall. Beams of runaway electrons may occur in this phase and hit the wall with high energy densities. They are not considered here as a main source for gross erosion losses.

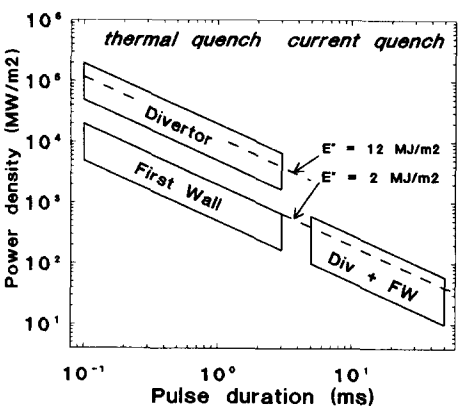

Fig. 1. Energy deposition on ITER plasma facing components due to plasma disruptions (excl. runaway electrons).

A total number of 500 disruptions at full power is foreseen for the Physics Phase and 200 for the Technology Phase. During the Physics Phase an additional 1000 disruptions are anticipated at reduced plasma parameters, with thermal energy about 1/3 of the full power case. The thermal quench for this case will be much softer, but the current quench is similar to the full power case. Energy depositions on the divertor plate may occasionally be similar as for the full power thermal quench [3].

In the present paper carbon is considered as the primary choice for Plasma Facing Components (PFC) armour in the ITER Physics Phase and tungsten for the Technology Phase, with beryllium as a back-up option for both [2]. The lifetime estimates only concern the number of hard disruptions (i.e. at full power).

2. Numerical results

2.1. Material properties

Calculations for the melting and evaporation behaviour have been performed by the ITER partners: United States (US), Japan (J), Soviet Union (SU) and European Community (EC) for carbon, tungsten and beryllium, see e.g. [4–12]. Figures 2a–c, 3a–c and table 1 contain the main thermophysical properties as used for the calculations by the different parties.

Different assumptions have been made for the conductivity of carbon, see fig. 2a. Japanese calculations were based on CX-2002U Carbon Fiber Composite (CFC) material, [7], US used data of pyrolytic graphite for the divertor case and graphite Graphnol N3M (similar to graphite H-451) for the First Wall [4–6], SU used data that were preliminary presented by US during the CDA of ITER [8]; EC results were mainly obtained with graphite H-451 conductivity values and parametric studies were performed for carbon materials with higher conductivity [9–12]. A major difference between US, J, SU and EC concerns also the carbon properties at temperatures exceeding 3500 °C, figs. 2a, 3a and table 1. Since the molecular cluster size of carbon vapor increases with temperature, EC takes evaporation energy $H_{ev} \sim 23$ kJ/g (average vapor composition mainly C_3 molecular carbon clusters) while US, J and SU have $H_{ev} \sim 60$ kJ/g (mono-atomic evaporation).

Clear discrepancies concern the data for tungsten (see figs. 2b, 3b and table 1). The J data for tungsten conductivity differ strongly (20% higher for the average over 0–3500 °C) from US, SU and EC data, which are close to values recommended by the Thermophysical Properties Research Center [13]. For the heat capacity, fig. 3b, the EC data are more conservative as compared to US, J data are in between.

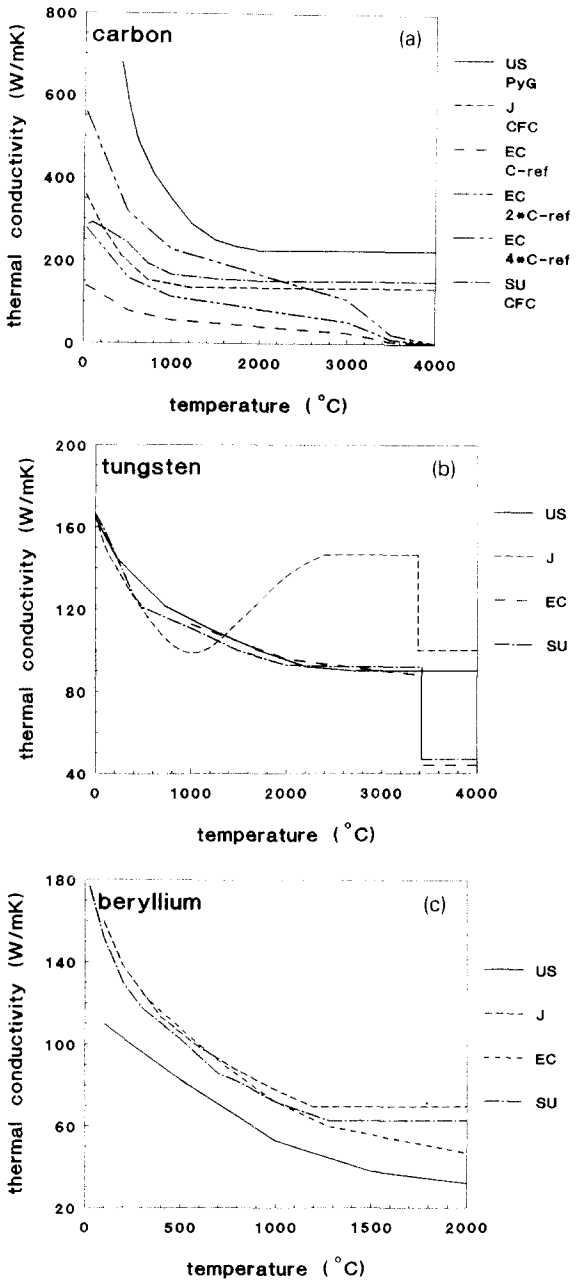

Fig. 2. Conductivity values used in thermal calculations: (a) carbon, (b) tungsten, (c) beryllium.

Beryllium data (see figs. 2c, 3c and table 1) of J, SU and EC are in good agreement, only J used lower value for heat of vaporization, (~ 70% of US, SU and EC). US used conductivity for beryllium alloy S65.

2.2. Evaluation of thermal response

Typical results from various codes for the thermal response of plasma facing materials to disruption heat fluxes are indicated in figs. 4a–d. The initial conditions were as follows:

US : Divertor: 10 mm pyrolytic graphite, 10 mm tungsten or 2 mm beryllium on 3 mm copper, heat flux ~ 10 MW/m^2 prior to disruption for divertor case [4,6].

J : CFC (CX-2002U), tungsten or beryllium at 500 ° C [7].

EC : CFC and tungsten at 1000 ° C, beryllium and some tungsten cases at 500 ° C [10,12].

SU : CFC and tungsten at 1000 ° C, beryllium at 500 ° C.

The results for carbon are given in fig. 4a, but the data have been processed for proper comparison: the calculated erosion is multiplied by a factor 5.1 (US), 5.2 (J), 4.9 (SU) and 2 (EC) respectively, to accomodate for experimental data; see the discussion below. For carbon there is a reasonably good agreement between parties, the steeper slope of J and EC curves compared to US is due to material density, and the results for 3 ms reflect the differences in thermal conductivity more clearly.

The results for tungsten evaporation and a 0.1 ms pulse (fig. 4b, also the 3 ms case, not show here) of the partners are in reasonable agreement (similar slopes); the penetration of the melting front is different. The thicker melt layer in the J case might be explained by its higher conductivity. The onset of melting and evaporation in J case is higher than the others, due to higher conductivity.

For the beryllium 0.1 ms case the US, SU and EC results are very similar, shown in fig. 4c. For the J case the higher evaporation rate is mainly due to the significantly lower evaporation energy. This also affects the longer pulse case, 3 ms, given in fig. 4d. EC results for 1 ms and 5 ms (the latter not shown), are in reasonable agreement with US for evaporation rate as well as melting depth for $E'' < 5$ MJ/m^2. J (0.1 and 3 ms) and SU (3 ms) results show much deeper penetration of the melting front, probably due to the higher conductivity assumed for the molten layer.

3. Vapour shielding

The possible reduction of incident power during disruptions by the interaction of vaporized material with plasma has been well recognized for years, see Sestero [14]. Several models have been developed as by Sestero [15], Hassanein [16] and Gilligan [17] (reviewed by Bolt [18]), see the overview in table 2. However, no clear experimental evidence for this phenomenon has been obtained so far. Preliminary results with plasma discharge devices in the 0.1 ms regime in USSR [19], as well as in US [20] seem to indicate strong reduction of absorbed energy density as compared to the incident one. However, the results obtained cannot be applied directly to ITER conditions yet. This is due to lack of quantification of experimental parameters and because

Table 1
Main material properties

	US	J	SU	EC
Carbon				
Density (10^3 kg/m^3)	2.2	1.75	1.85	1.74
Heat of vaporization (kJ/g)	59.1	60	56.7	23
Tungsten				
Density (10^3 kg/m^3)	19.25	19.3	19.3	17.5
Melting point (° C)	3410	3380	3410	3410
Heat of fusion (kJ/g)	0.22	0.25	0.25	0.22
Heat of vaporization (kJ/g)	4.63	4.8	4.68	4.8
Beryllium				
Density (10^3 kg/m^3)	1.89	1.845	1.848	1.85
Melting point (° C)	1287	1280	1287	1280
Heat of fusion (kJ/g)	1.640	1.10	1.465	1.3
Heat of vaporization (kJ/g)	36	24.8	34.400	32.827

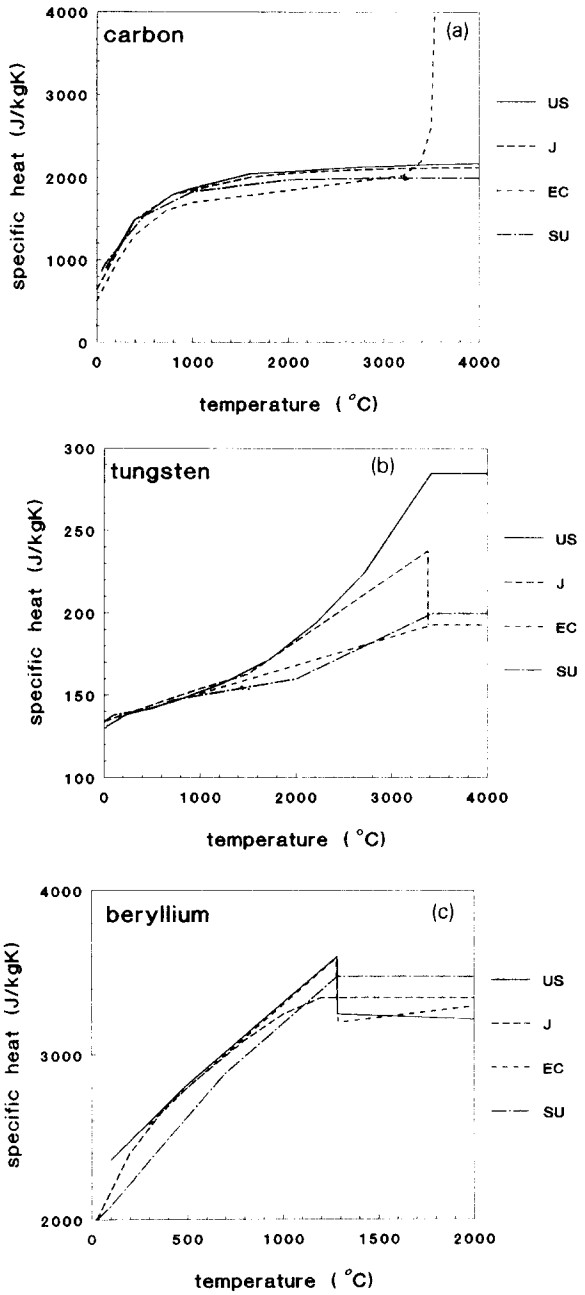

Fig. 3. Specific heat values used in thermal calculations: (a) carbon, (b) tungsten, (c) beryllium.

of different loading conditions as indicated in table 2. Related modelling work in USSR is in progress [21].

The vapour shield models in general result in a reduction of melt front penetration and significant reduced evaporation. An example is given in fig. 5 for a short pulse on tungsten. The evaporation curve in the Vapour Shield (VS) case (Hassanein model, [16]) at higher energy densities has a slope identical to the transmitted fraction (50%) of the ultimate value without VS (~ 5.6 μm/MJ/m^2 versus 11.3 μm/MJ/m^2). The effect on erosion for $E'' = 12$ MJ/m^2 is about a factor 2 reduction, for E'' around the melting and evaporation thresholds the reduction of evaporation by VS is much more pronounced.

4. Comparison of experimental results

The amount of experimental data on short pulse disruption erosion is most extensive on carbon materials [7,10,12,22–26]. No test results by laser or electron beam are available on tungsten and beryllium. Therefore in this section only results on carbon will be discussed.

As mentioned above, the observed erosion of carbon in short pulse laser and electron beam experiments has been reported to be up to a factor 2 higher than predicted, assuming vapor composed mainly of C_3 molecular carbon clusters ($H_{ev} \sim 23$ kJ/g), or a factor 5, assuming overall mono-atomic evaporation ($H_{ev} \sim 60$ kJ/g) [7,10,12]. This fact has been accounted for in the disruption erosion lifetime estimates for PFC in the ITER CDA [2]. In fact, for longer pulses and lower power density the effective H_{ev} is about 20–25 kJ/g ($P'' = 300$–350 MW/m^2 during 20–50 ms with electron beam [22,23], $P'' = 300$–1000 MW/m^2 during 10–20 ms with laser [10,12]). An increase of thermal erosion with increasing power density (> GW/m^2) and decreasing pulse duration (< 5 ms) has been found, leading to an effective H_{ev} of 10–15 kJ/g (Occasionally 5–20) [22,25]. A clear contribution from particle emission to the erosion process has been identified by photography and high speed video techniques [25,26].

Results from short pulse heat flux experiments on carbons by JEBIS (JAERI (Japanese Atomic Energy Research Institute) Electron Beam Irradiation Stand) and laser (Forschungszentrum Jülich, FRG (KFA) & Energieonderzoek Centrum Nederland, Petten, NL (ECN)) have been compared quantitatively. For this purpose mainly the data given in [12,22–25] have been considered, which were obtained on a number of graphite materials and CFC's with a pulse duration of 5 ms, see table 3. In fig. 6a–b a typical result is given as measured erosion depth versus energy density and a compilation of erosion depth data at 5 ms is given in fig. 7a–b. Data deduced from mass loss measurements were not considered since the conversion to erosion

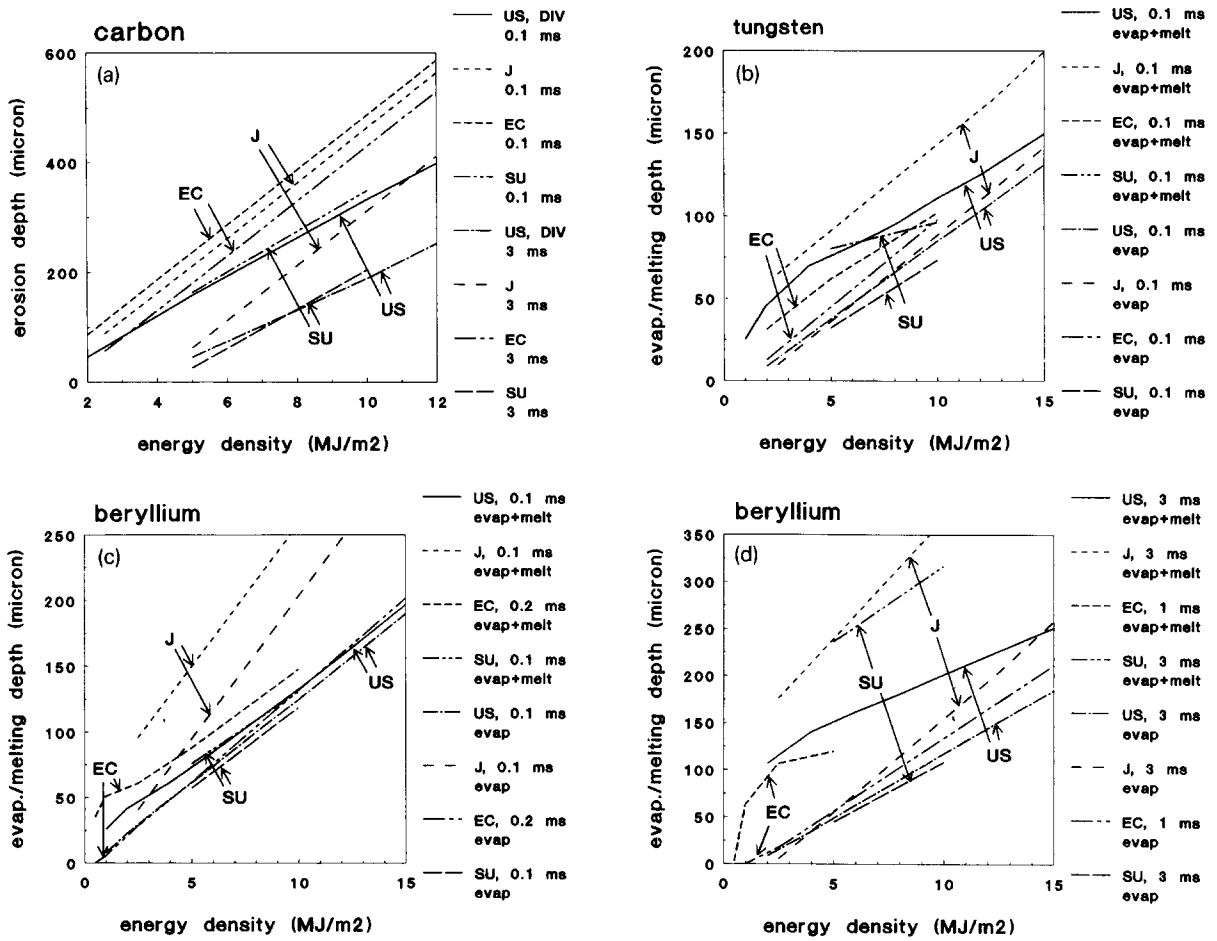

Fig. 4. Calculated thermal response due to energy deposition in 0.1–3 ms. For carbon only the evaporation is given, for tungsten and beryllium both the depth of melting front and surface recession by evaporation are given: (a) carbon, 0.1–3 ms; (b) tungsten, 0.1 ms; (c) beryllium, 0.1 ms; (d) beryllium, 3 ms.

depth is not direct but by a factor 2–5 depending on crater geometry, and is subject to error e.g. by redeposition of material. For the purpose of comparison typical conductivity values for each material were averaged over the temperature range from 20 to 1000 °C, see table 3 [25,26]. In the same figures (6a–b, 7a–b), car-

Table 2
Main characteristics of vapour shield models and anticipated ITER conditions

Item	Hassanein	Sestero	Gilligan	ITER thermal quench
Incident energy	ions	plasma	radiation (2–5 eV)	plasma (conv./cond./rad.) ($T_{edge} < T_{disr} < T_{core}$)
Vapour cloud:				
ionization	no	yes	yes	yes
transport	no	yes	no	yes
optical properties	transparent	thin	thick	?
B-field	no	$\perp$	$\parallel$	grazing
Transmitted energy fraction	0.5	~ 0.3	0.05–0.2	??

bon erosion in 5 ms pulses has been calculated parametrically with a material density of 1.7 and 2.2 g/cm^3, and conductivity of H-451 multiplied by factors 0.5, 1, 2, 4 and 8, which covers all materials of interest [12]. Figures 7a–b show that the erosion by tests with JEBIS and both Nd:YAG-laser facilities at $E'' = 6$ and 9 MJ/m^2 is roughly between 0.7 and 2.5 times the predicted value. The results of ECN are closer to prediction, partly lower. For $E'' = 9$ MJ/m^2 the laser values are in general lower than the JEBIS results except for CL A05 ||. Concerning the data trends for $E'' = 6$–9 MJ/m^2, the results at 9 MJ/m^2 are lower than expected from the $E'' = 6$ MJ/m^2 results, especially for the laser tests. Several aspects may play a role here. For the smaller spot size in laser experiments the radial heat conduction may be significant. Also, in the laser case the absorbed energy density has been considered, which is about 90% of the incident one. Another difference between EB and laser is due to the fact that the energetic electrons penetrate 50–100 μm into the material, which gives a different near-surface temperature profile. Microstructural features for tests by EB and laser seem to be similar for graphites and felt type CFC, and differ somewhat for pyrolytic carbon and multidirectional CFC, e.g. for Pfizer Pyroid the surface shows deep pits with EB while it is smooth by laser [24]. A detailed evaluation of the relation between beam profile and crater geometry has not been made yet, which due to radial heat flow effects leaves an uncertainty in the energy density E''. All erosion depth results from laser tests by KFA are higher than the laser data from ECN. One reason is that in the KFA case the laser beam has been assumed to have a top hat intensity distribution, while ECN accounted for a peaking of about 20%. Another difference is that the ECN experiments have been performed in high vacuum on outgassed specimens, while KFA-ILT tests were performed at atmospheric pressure and inert gas environment; also part of the JEBIS tests have been performed on non-outgassed specimens. The effect of non-outgassing on erosion may both have a chemical aspect as well as a mechanical due to high gas pressures in the pores of the material.

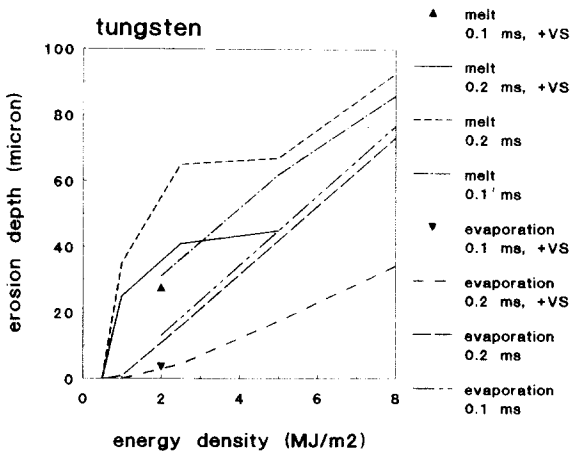

Fig. 5. Calculated thermal response due to energy deposition in 0.2 ms for tungsten, including vapor shielding of 50% maximum. Both the depth of melting front and surface recession by evaporation are given.

Cracking of Pfizer Pyroid has been observed in both

Table 3
Thermal conductivity and density values for materials shown in figs. 6 and 7. Conductivity is averaged over the temperature range 0–1000 °C. (+/−: test result yet/not available)

Material	Density (g/cm^3)	Av. Cond. (W/mK)	JEBIS	KFA laser	ECN laser
Dunlop DMS 678 ⊥	1.73	50	−	−	+
V1325	1.89	55	+	+	−
LCL A05 ⊥	1.8	60	+	+	+
EK-98	1.86	70	+	+	−
POCO AXF 5Q	1.83	75	+	+	−
IG-430	1.8	80	+	−	−
H-451	1.73	90	−	−	calc.
FMI 3-3-3-3	1.9	110	+	+	−
Dunlop DMS 678 ‖	1.73	120	−	−	+
Sepcarb N112 ‖	1.95	125	−	−	+
LCL A05 ‖	1.8	150	+	+	+
CX2002U	1.7	160	+	−	−
Pfizer Pyroid ‖	2.2	325	+	+	+
ECPG	2.25	420	−	−	+

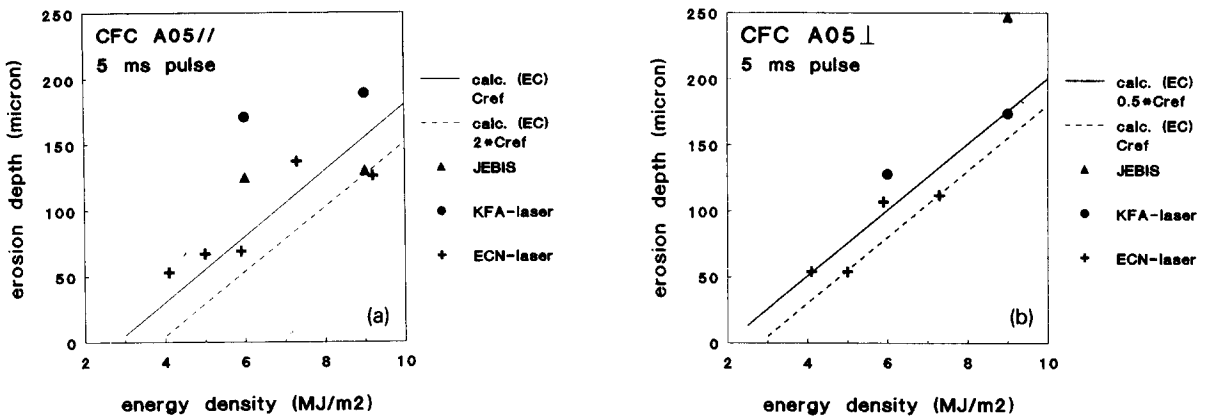

Fig. 6. Experimental data on carbon materials by laser on electron beam tests, 5 ms pulses. Calculated curves based on $H_{ev} = 23$ kJ/g. (a) LCL A05 ||, (b) LCL A05 ⊥.

types of tests: at $E'' \sim 6$ MJ/m^2 in 5 ms for JEBIS and $E'' \sim 8$ MJ/m^2 at 10 ms resp. $E'' \sim 1$ MJ/m^2 at 0.2 ms by laser.

5. ITER Plasma Facing Components (PFC) lifetime estimates

Lifetime estimates of ITER PFC have been performed for the reference disruption scenario. Cases considered for the divertor are:

- 6 mm CFC (A05 or CX2002U) and 12 mm high conductivity CFC or pyrolytic graphite (PyG, density 2.2 g/cm^3) with 5 and 10 mm sacrificial layer thickness respectively.
- 2 mm sacrificial Be or W.

For PyG the US calculations have been used, for CFC the J ones, for W and Be the US ones. The disruption lifetime has been evaluated for 0.1 and 3 ms pulse duration and 12 MJ/m^2 incident energy density, without considering the effects of separatrix sweeping. Material losses considered: evaporation + entire removal

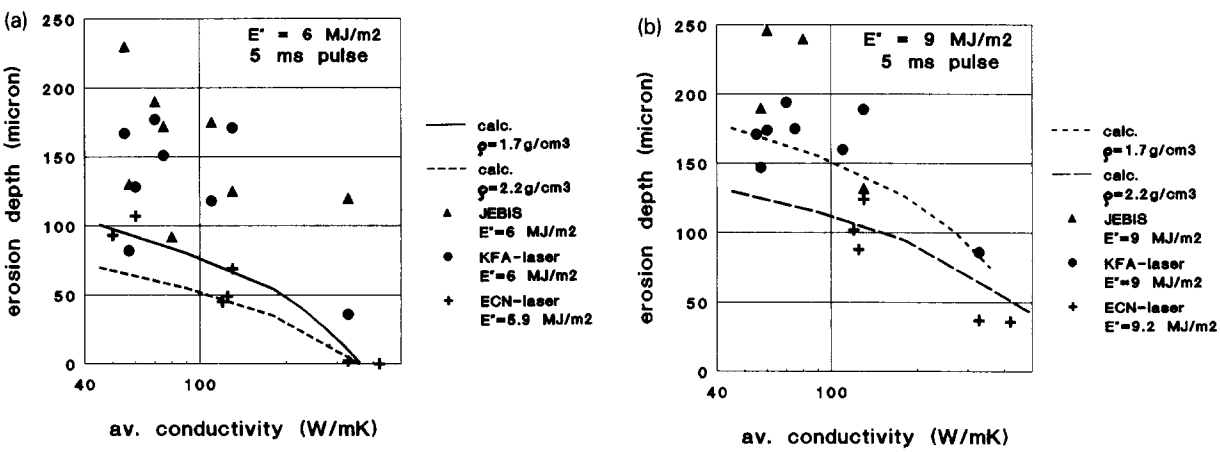

Fig. 7. Compilation of experimental data from JAERI (JEBIS), KFA-ILT (Nd:YAG laser) and ECN (Nd:YAG laser). The calculated erosion is shown as a function of the average value of thermal conductivity in the range 0–1000 °C, for a material density of 1.7 and 2.2 g/cm^3 (data given in table 3). As an example: on the x-axis the H-451 type material has an average conductivity of 90 W/mK and Pfizer Pyroid 320 W/mk. Note that calculated curves are based on $H_{ev} = 23$ kJ/g. (a) $E'' = 6$ MJ/m^2, (b) $E'' = 9$ MJ/m^2.

of melt; evaporation + half of melt layer removed; evaporation only; evaporation reduced (vapour shield 50%), see table 4.

The most conservative estimates of the number of allowed disruptions (loss of melt layer) are similar for Be (9–13), CFC (9–12) and W (7–16); PyG would survive 26–42 disruptions. In a more realistic estimate (vapor shield) tungsten would survive up to twice as much disruptions (39–62) as beryllium (26–28) or CFC (18–24). PyG would survive about 2–3 times more disruptions (52–83) than Be or CFC.

For the first wall the following cases are considered: sacrificial armour thickness of 10 mm for CFC (with conductivity equal to H-451) and thin coatings of 0.5 mm for W&Be. Material losses considered are: entire removal of melt, evaporation only, evaporation reduced by vapour shield. The results for an energy density of 2 MJ/m^2 are given in table 5. For CFC the armour survives at least 125 disruptions in a worst case (0.1 ms), up to at least 500 for a slower disruption (3 ms).

The melt layer thickness in the Be and W cases is relatively larger than the evaporation depth as compared to the divertor case. This leads to a much wider range of lifetime estimates. Estimated minima, assuming melt layer losses, are about 10 for Be and 15 for W. If only evaporation occurs, a Be coating would survive 25–250 disruptions and W at least 50. W is unaffected by the soft 3 ms deposition duration.

The additional effect of the energy deposition in the current quench (2–3 MJ/m^2, 5–50 ms) has not been considered yet in detail by all parties. The worst case (for surface damage) would arise for the case of the shortest current quench duration, since its energy deposition follows immediately on the thermal quench, in which case the surface will already be very hot and in the metal case have a molten surface layer. The subsequent energy deposition at a lower power density, will cause deeper penetration of the melting front [8,9]. The melt layer is much less stable when the forces acting have more time and deformation or movement of the layer is likely to happen [31,32].

Table 4
Disruption erosion lifetime estimate for divertor plate (US-calc. for Be, PyG and W, J-calc. for CFC); low/high: lowest/highest value for 0.1 or 3 ms pulse duration

	evap. + melt	evap. + ½melt	evap. only	evap. (+VS)
CFC				
low			8.9	17.7
high			12.1	24.3
PyG				
low			25.8	51.5
high			41.7	83.3
Tungsten				
low	7.1	11.5	19.4	38.8
high	16	17.5	30.8	61.5
Beryllium				
low	9	10.9	13.2	26.4
high	12.7	12.9	13.8	27.6

Table 5
Disruption erosion lifetime estimate for first wall armour (average of US/EC-calc. for Be and W, with vapour shield (VS): EC-calc., EC-calc. for CFC)

CFC	exp.	calc.
0.1 ms (+VS)	250	500
0.1 ms	125	250
1 ms	167	334
3 ms	550	1100
Tungsten	evap. + melt	evap. only
0.1 ms (+VS)	18	250
0.1 ms	13	50
1 ms	14	500
3 ms	∞	∞
Beryllium	evap. + melt	evap. only
0.1 ms (+VS)	12	56
0.1 ms	12	23
1 ms	8	42
3 ms	6	250

6. Discussion

The lifetime estimates for ITER divertor presented in table 5 imply that for the ITER Physics phase (500 full power disruptions) frequent replacement or repair is needed. For a 5 mm sacrificial CFC armor, with an estimated lifetime of 10–25 disruptions, very frequent replacement is needed. In case of a higher thermal conductivity material the allowable sacrificial layer thickness will increase. A realistic limit for high conductivity CFC seems to be about 10 mm, similar to the case of pyrolytic graphite (for 1000 °C surface temperature in normal operation). In this case the replacement frequency would be 2–3 times lower. The effect of degradation of thermal conductivity by neutron damage is not considered here, partly because of the estimate that the surface recession by disruption erosion seems to appear faster [33]. In case of beryllium, for which in-situ repair by plasma spray could be an alternative, a high number of repair actions would be needed. This number may be even increased if the

coating conductivity would be lower compared to the dense metal values.

A CFC first wall (FW) armour in the Physics Phase is likely to survive or only need marginal replacement if about 15 mm erosion thickness would be available. The thin Be coated FW needs repair after each 10 disruptions if the melt layer would be removed but would survive 30–250 disruptions if the mass loss is by evaporation only. A main improvement here results if the sacrificial layer thickness could be enhanced by a factor 5 or more.

Another point of consideration is the expectation that the plasma disruption will not hit the same spot repeatedly. For the divertor, where X-point sweeping of ± 15 cm is foreseen, the effective reduction in erosion might be up to 50% for the fast phase erosion (essentially equal to the time average of peak heat flux in normal operation, with widened profile). For the first wall a wider scatter in the location of the disruption hot spot is likely to occur, which would reduce the maximum surface recession by a larger factor.

As pointed out by Bolt [18,34] the thermal erosion in a disruption may be reduced by nearby redeposition, due to rapid ionization of evaporated material and transport along the grazing field lines. This effect of redeposition/recycling is yet unknown as is the vapour shield, but may have a strong impact on the present considerations. On this subject, no further analyses or experimental results are available which would allow for quantitative statements yet. Also the metal evaporation and melt layer thickness is affected if convection processes occur in the melt layer, which will increase the melt layer thickness, but decrease the evaporation [9].

To increase the PFC lifetime in ITER operation, it will be necessary to employ disruption control mechanisms already during the start of the Physics Phase. Their development is the subject of ITER R&D activity [35]. Slowing down of energy deposition in the thermal quench will be beneficial for carbon, but may be not for beryllium, where severe melting occurs.

7. Conclusions

- The material response to disruption heat loads as calculated by different codes, shows reasonable agreement, considering the different initial assumptions and material properties used. For carbon this agreement is rather good. For beryllium and tungsten US and EC data are similar, on the other hand J data show in general a much thicker melt layer.
- A comparison of vapour shield models shows large differences in shielding efficiency. Since none of the models covers the expected ITER conditions properly, a reliable statement on the actual vapour shielding factor cannot be given. For lifetime estimates the more conservative vapour shield model (50% maximum shielding) is recommended for the purpose of comparison.
- Experimental data for simulated disruption erosion of carbon materials by laser and electron beams have been compared and show agreement with each other roughly within a factor 2. The derived effective evaporation energy varies from 20–25 kJ/g for power densities of the order of 500 MW/m^2 and pulse duration 10–50 ms, to 10–15 kJ/g (occasionally 5–20), for power densities exceeding 1000 MW/m^2 and pulse durations less than 5 ms. This is due to the increasing size of molecular vapor species and gross particle emission.
- In order to improve the correlation of the heat flux experiments with the numerical predictions the measurement of surface temperatures will be needed and effects of radial heat flow and time dependence should be evaluated. Beam profile characterization and erosion crater measurements should be correlated by appropiate 2-D thermal calculations.
- Lifetime estimates for the ITER PFC depend very strongly on the assumed material loss mechanisms. A wider range as in the ITER-report [2] has been considered and some calculations have been revised. The lifetimes estimates are based on the erosion in the thermal quench and vary roughly between 10–80 disruptions for a carbon divertor (not considering X-point sweeping) and 125 to more than 500 for a carbon armoured first wall.
- The lifetime estimates are strongly dependent on the energy deposition parameters given by plasma physics considerations as e.g. the width of the scrape-off layer during disruptions and energy deposition duration. More information on these effects in present machines is clearly needed.

Acknowledgement

The authors want to thank G. Pacher (NET), H. Ise (JAERI), A. Benz (KFA), H. Klippel (ECN) and R. van der Stad (ECN) for their contributions and comments.

References

[1] D.E. Post (ed), ITER Physics, ITER Documentation Series, No. 21, Chapter 4 (IAEA, Vienna, 1990).

[2] T. Kuroda, G. Vieider (eds), ITER Plasma Facing Components, ITER Documentation Series No. 30 (IAEA, Vienna, 1990).
[3] G.W. Pacher, NET-Team, Garching, private communication.
[4] A. Hassanein, in: US-contribution to the ITER Plasma Facing Components Engineering Homework Task (June 1989).
[5] A. Hassanein, Disruption analysis for the divertor plate, in: US Contribution to ITER PFC Homework (January 1990) ITER-TN-PC-1-0-U-1.
[6] A. Hassanein, First wall disruption analysis, in: US contribution to ITER PFC Homework (January 1990) ITER-TN-PC-1-0-U-1.
[7] T. Kuroda, M. Seki, S. Yamazaki, Estimates of erosion thickness of divertor surface materials during plasma disruptions, in: Japanese contribution to ITER Joint Work (June–October, 1989).
[8] I. Mazul (ed.), Divertor target, in: USSR Contribution to ITER Working Session (Jan. 1990).
[9] H.Th. Klippel and R.C.L. van der Stad, Thermal analysis of plasma disruptions on first wall (FW) and divertor, ECN-C-90-003 (Dec. 1989).
[10] J.G. van der Laan, H.Th. Klippel, R.C.L. van der Stad and J. Bakker, Experimental simulation and analysis of off-normal heat loads accompanying plasma disruptions, in: Proc. 15th Symp. on Fus. Tech., Sept. 3–7, London, 1990 (Elsevier, Amsterdam, 1991).
[11] H.Th. Klippel, R.C.L. van der Stad, New Calculations on Surface Erosion Resulting from High Energy Density Plasma Disruptions on Plasma Facing Components, ECN report, in preparation.
[12] J.G. van der Laan, H.Th. Klippel, J. Bakker and R.C.L. van der Stad, Simulation and Analysis of the Response of Plasma Facing Materials to Off-Normal Heat Loads accompanying Disruptions, ECN report in preparation.
[13] C.Y. Ho, R.W. Powell and P.E. Liley, Thermal conductivity of the elements: a comprehensive review, J. Phys. Chem. Ref. Data 3 (1974) Suppl. No. 1, I-690.
[14] A. Sestero, Protection of walls from hard disruptions in large tokamaks, Nucl. Fusion 17 (1977) 115–123.
[15] A. Sestero and A. Ventura, Formation and Evolution of 'Virtual Limiters' in hard Disruptions, NET-Report EUR XII 324–24.
[16] A.M. Hassanein, G.C. Kulcinski and W.G. Wolfer, Surface melting and evaporation during disruptions in magnetic fusion reactors, Nuclear Engrg. Des./Fusion 1 (1984) 307–324.
[17] J. Gilligan, D. Hahn and R. Mohanti, Vapor shielding of surfaces subjected to high heat fluxes during a plasma disruption, J. Nucl. Mater. 162–4 (1989) 957–963.
[18] H.H. Bolt, Evaluation process of the thermal erosion during disruptions for ITER, US–Japan Workshop P-165, Nagoya (Dec. 1990).
[19] V.R. Barabash et al., Damage of refactory metals and carbon-based materials under simulation of the thermal influence at plasma disruption, ISFNT-2, Karlsruhe 1991, Fusion Engrg. Des. 18 (1991) 145–150, in these Proceedings, Part C.
[20] J. Gilligan et al., Studies of high heat-flux and runaway electron damage on plasma-facing materials, J. Nucl. Mater 176&177 (1990) 779–785.
[21] V. Kozhevin, Efremov Institute Leningrad, private communication (July 1991).
[22] M. Akiba, T. Kuroda, M. Seki et al., JEBIS&KHI test results IG430, CX2002U, J contrib. to ITER, private communication (March 1991).
[23] M. Araki, M. Akiba, H. Ise, M. Dairaku, K. Yokoyama and M. Seki, High heat flux experiments of CFC and graphite materials for fusion applications, in: Proc. International Symposion on carbon, Tsukuba, November 1990, 210–213.
[24] J. Linke, M. Akiba, M. Araki et al,, Disruption simulation experiments in electron & laser beam facilities, Proc. 15th Symp. on Fus. Tech., Sept. 3–7, London, 1990 (Elsevier, Amsterdam, 1991).
[25] J.G. van der Laan and H.Th. Klippel, Simulation and analysis of the response of carbon materials to off-normal heat loads accompanying plasma disruptions, J. Nucl. Mater. 179–181, Part A (1991) 184–188.
[26] M. Akiba, JAERI, private communication (December 1991).
[27] E.P. Roth, R.D. Watson, M. Moss and W.D. Drotning, Thermophysical Properties of Advanced Carbon Materials for Tokamak Limiters, Sandia Report, SAND88-2057 (April 1989).
[28] M. Yamamoto, T. Ando, H. Takatsu et al., Evaluation tests on First Wall and Divertor Plate Materials for JT-60 Upgrade, JAERI Report, JAERI-M 90-119 (August 1990).
[29] J.P. Bonal, PPM1-2 Pre-Irradiation Progress Report Petten 2 Experiment, CEA report SECS/LMA/90-NT-39 (1990).
[30] B. Thiele, Pre-Irradiation Material Characterization and Loading Report on Neutron Irradiation Tests GRIPS and CERAM D217, KFA Report IRW-TN-39/90 (July 1990).
[31] A.M. Hassanein, Stability and erosion of melt layers formed during plasma disruptions, Fusion Technol. 15 (1989) 513–521.
[32] H. Madarame, T. Sukegawa and K. Okamoto, A simulated plasma disruption experiment using a magneto-plasma-dynamic arcjet, ISFNT-2, Karlsruhe 1991, Fusion Engrg. Des. 18 (1991) 109–116, in these Proceedings, Part C.
[33] M.I. Budd, Estimated influence of neutron damage on the divertor plate protection material during the physics phase of NET, J. Nucl. Mater. 170 (1990) 129–133.
[34] H.H. Bolt, Y. Ooishi, M. Iida and T. Sukegawa, Study of the plasma–material interaction during simulated plasma disruptions, ISFNT-2, Karlsruhe 1991, Fusion Engrg. Des. 18 (1991) 117–123, in these Proceedings, Part C.
[35] C. Flanagan (ed), R&D Needs for ITER Engineering Design, ITER Documentation Series, No 20 (IAEA, Vienna, 1990).